A simple optical index shows spatial and temporal heterogeneity in plankton community composition during the 2008 North Atlantic Bloom

I. Cetinić[1], M. J. Perry[1], E. D'Asaro[2], N. Briggs[1], N. Poulton[3], M. E. Sieracki[3,*] and C. M. Lee[2]

[1]{Ira C. Darling Marine Center, School of Marine Sciences, University of Maine, Walpole, Maine, USA}

[2]{Applied Physics Laboratory and School of Oceanography, University of Washington, Seattle, Washington, USA}

[3]{Bigelow Institute for Ocean Sciences, East Boothbay, Maine, USA}

[*]{now at: National Science Foundation, Arlington, VA, USA }

Correspondence to: I. Cetinić (icetinic@gmail.com)

Abstract

The ratio of two *in situ* optical measurements, chlorophyll fluorescence (*Chl F)* and optical particulate backscattering (b_{bp}), varied with changes in phytoplankton community composition during the North Atlantic Bloom experiment in the Iceland Basin in 2008. Using ship-based measurements of *Chl F,* b_{bp}, chlorophyll *a (Chl*), HPLC pigments, phytoplankton composition and carbon biomass, we found that oscillations in the ratio varied with changes in plankton community composition; hence we refer to *Chl F*/b_{bp} as an "optical community index". The index varied by more than a factor of two, with low values associated with pico- and nanophytoplankton and high values associated with diatom dominated phytoplankton communities. Observed changes in optical index were driven by taxa-specific chlorophyll-to-autotrophic carbon ratios and by physiological changes in *Chl F* driven by the silica limitation. A Lagrangian mixed-layer float and four Seagliders, operating continuously for two months, made similar measurements of the optical community index and followed the evolution and later

demise of the diatom spring bloom. Temporal changes in optical community index and, by implication the transition in community composition from diatom to post-diatom bloom communities, were not simultaneous over the spatial domain surveyed by the ship, float and gliders. The ratio of simple optical properties measured from autonomous platforms, when carefully validated, provides a tool for studying phytoplankton patchiness on extended temporal scales and ecological relevant spatial scales, and should offer new insights into the processes regulating patchiness.

1 Introduction

Autonomous observations of phytoplankton are becoming increasingly ubiquitous, including *in situ* optical sensing from Argo-type and Lagrangian floats, gliders, and moorings, as well as remote sensing from space. Phytoplankton biomass is assessed through several different optical proxies including *in situ* chlorophyll *a* fluorescence (*Chl F*; Lorenzen, 1966), phytoplankton absorption coefficient ($a_{phy}(\lambda)$) or particulate absorption coefficient in waters dominated by phytoplankton (Bricaud et al., 1995; Roesler and Barnard, 2014), and chlorophyll derived from *in situ* or remotely-sensed ocean reflectance at visible wavelengths (O'Reilly et al., 1998). High-frequency optical measurements are ideal for detecting temporal change and spatial patchiness, and in improving understanding of the role of meso- and submeso-scale physics on the distribution of phytoplankton in the ocean (Denman and Platt, 1976; Yoder et al., 1987; Munk, 2000). Autonomous optical observations have enabled advances in understanding the timing of and mechanisms responsible for initiating blooms (Perry et al., 2008; Boss and Behrenfeld, 2010; Ryan et al., 2011; Mahadevan et al., 2012; Matrai et al., 2013).

Less common, more challenging, but increasingly important are autonomous measurements of phytoplankton community composition. Knowledge of the community composition is critical to understanding and predicting vital ecosystem functions such as carbon flux and efficiency of carbon transfer to higher trophic levels (biomass is not enough), particularly as the oceans change in response to climate change and ocean acidification. A few direct autonomous measurements of phytoplankton community composition have been made, but only on moorings due to the high power consumption of the flow or imaging-in-flow cytometric sensors (Olson and Sosik, 2007; Sosik and Olson, 2007; Campbell et al., 2013). A diversity of satellite-based

algorithms for determining phytoplankton functional types from ocean color reflectance has been developed in the last decade (see review of Moisan et al., 2012), although without community consensus as to robustness. Nencioli et al. (2010) implied that changes in the ratio of *Chl-to*-particulate beam attenuation coefficient (c_p) and the backscattering ratio (b_{bp}/b_p, where b_{bp} is total particulate scattering coefficient and b_p is backscattering coefficient) are associated with changes in phytoplankton composition and physiological (light) adaptation in eddies off Hawaii. In a mooring study of the spring bloom in the Labrador Sea, change in phytoplankton species composition is offered as the explanation for the observed variability in *Chl F*/c_p, although this suggestion is unconfirmed by *in situ* measurement of species composition (Strutton et al., 2011).

In this study we define an "optical community index" as the ratio *Chl F*-to-b_{bp} and connect it to plankton community composition using ship-based measurements of *Chl F,* b_{bp}, HPLC pigments, phytoplankton composition, and carbon biomass during two cruises to the Iceland Basin. For two months during the 2008 North Atlantic Bloom experiment (NAB 2008), we used a Lagrangian float as the reference frame to track the initiation of the diatom bloom in mid-April, through depletion of silicic acid and bloom termination in mid-May. The optical index, *Chl F*/b_{bp}, varied as a function of plankton community composition, decreasing by a factor of two as the early diatom spring bloom community transitioned into a recycling community dominated by smaller pico- and nanophytoplankton (Cetinić et al., 2012). Rigorous cross-calibration of optical sensors amongst all platforms enabled us to project the optical community index to data collected by four Seagliders to construct a spatial time series of the evolution of phytoplankton community structure and to document its spatial heterogeneity. This approach, of using simple optical measurements validated with more expensive ship-based measurements, allows projection of the ship measurements to broader temporal and spatial scales.

2 Material and methods

2.1 Study site and platforms

A Lagrangian float and four Seagliders were deployed near the JGOFS NABE 60ºN site (Ducklow and Harris, 1993) from the *R/S Bjarni Saemundsson* on yearday, YD, 95 (4 April 2008; Fig. 1; (Briggs et al., 2011; Alkire et al., 2012; Mahadevan et al., 2012). The float tracked

the horizontal motion of the mixed layer for almost two months, until the end of its mission on YD 146 (25 May 2008). An extensive discussion of the evolution of the bloom in the patch tracked by the float is provided in Alkire et al. (2012). The gliders were piloted to survey an approximately 50 km region around the float. Depending on currents and eddies, they occasionally swept further away (up to 175 km from the float). By the end of the float deployment in late May, they operated within 50 km of the float. A water sampling and sensor inter-calibration cruise on the *R/V Knorr* occurred between YD 123 –142 (2 – 21 May 2008), when the ship surveyed waters in proximity of the float and gliders.

The Lagrangian float, designed and built at the University of Washington Applied Physics Laboratory, was similar to the MLFII model described in D'Asaro (2003). The float's deployment and sampling strategy, detailed in Alkire et al. (2012), were designed to mimic the motion of plankton, drifting within the mixed layer; once per day (~ 15 UTC) it profiled from the surface to a depth of ~ 230 m, returning thereafter to the mixed-layer drift mode. The float measured temperature and conductivity with two CTD sensors (Sea-Bird Electronics, Inc., SBE 41), one near the top and another near the bottom of the platform (see list of measured parameters and associated methods in the Table 1). A WET Labs FLNTU mounted at the bottom of the float measured *Chl F* (λ_{ex}=470 nm, λ_{em}=700 nm) and optical backscattering (λ=700 nm) at an angle, θ, of 140°. Photosynthetically active radiation, PAR (400 – 700 nm), was measured by a downwelling cosine PAR sensor (LI-COR 192-SA) mounted at the top of the float.

Seagliders, autonomous underwater vehicles designed for long ocean deployments, move forward horizontally while gliding vertically in a sawtooth pattern (Eriksen et al., 2001). Four Seagliders (SG140, SG141, SG142 and SG143) were deployed during this experiment, with an adaptive mission to follow the Lagrangian float on its path and provide measurements on larger spatial scales and to depths of 1,000 m. All gliders were equipped with an unpumped custom Sea-Bird Electronics, Inc., CT sensor that measured conductivity and temperature and carried a WET Labs BB2F that measured backscattering at two wavelengths (470 and 700 nm; θ=124°) and *Chl F* (λ_{ex}=470 nm, λ_{em}=700 nm).

Extensive surveys around the float and glider deployment area were carried out during a three-week process cruise aboard the *R/V Knorr*, with 134 CTD profiles. The CTD rosette was equipped with a Sea-Bird Electronics, Inc., SBE 911*plus* CTD. A WET Labs FLNTU (similar to

that on the float) was mounted on the bottom of the frame. A Biospherical QSP2300 sensor mounted on the top of the CTD rosette frame measured scalar underwater PAR. The same set of optical sensors was used during the short, six-day deployment cruise aboard the *R/S Bjarni Saemundsson*; fewer profiles and samples were collected during this cruise (9 CTD profiles).

All data used in this paper and the cited calibration reports are available under the project name NAB 2008 from the Biological and Chemical Oceanography Data Management Office (BCO-DMO, at http://osprey.bcodmo.org/project.cfm?flag=view&id=102&sortby=project).

2.2 In situ optical measurements and sensor inter-calibration procedure

Chl F and b_{bp} were measured on the float, four gliders and ship, with a total of six sensors (two FLNTUs and four BB2Fs). The ship's FLNTU was used as the primary reference sensor to which the autonomous sensors were brought into alignment via *in situ* inter-calibrations. All sensors were factory calibrated before and after the cruise *en masse* (with the exception of sensors on SG142, which was not retrieved). Dark readings (voltage) for both channels of the ship's FLNTU sensor were measured *in situ* by covering the detector window with black electrical tape on two profiles to 600 m, as suggested by Twardowski et al. (2007); these *in situ* dark measurements agreed with the mean factory dark volts. Prior to inter-calibration, mean pre- and post-deployment factory calibrations were applied to all sensors to convert *Chl F* into nominal *Chl* concentration and scattering measurements to the volume scattering function, $\beta_{total}(\theta, 700\ nm)$, which was converted to b_{bp} as follows. The volume scattering function of seawater, $\beta_{sw}(\theta, 700\ nm)$, calculated following Zhang et al. (2009), was subtracted from $\beta_{total}(\theta, 700\ nm)$ to yield the volume scattering function of particles, $\beta_p(\theta, 700\ nm)$, which was then converted to b_{bp} by multiplying $\beta_p(\theta, 700\ nm)$ by $2\pi\chi$, using χ factors of 1.132 for FLNTU and 1.077 for BB2F (Sullivan et al., 2013).

Offsets were applied to the factory calibrated glider data to bring the pre-bloom deep values for all gliders into alignment. The autonomous sensors were further aligned with ship sensors using matchups from intentional calibration stations, in which the float or glider was brought to the surface within close proximity to the ship and a CTD cast made as the vehicle descended. A total of 11 float casts and 2-3 casts per glider were made. Profiles were aligned in density coordinate space and ship profiles were interpolated to match the densities of the more sparse autonomous measurements, creating a ship-autonomous sensor matchup for every autonomous measurement

from each of the inter-calibration casts. Matchups from float inter-calibration casts were pooled to calculate a single linear regression for each sensor type (*Chl F* and b_{bp}), which were used to align float sensors to the ship. Matchups were insufficient to align each glider to the ship independently, so matchups from all four gliders (already aligned at depth) were pooled to calculate a single regression per sensor type, aligning all gliders with the ship as well. Finally, *Chl F* for all sensors was converted to volts, V (referenced to the ship's FLNTU). More details on the inter-calibration procedures are available in (Briggs et al., 2011) and in the reports available on BCO-DMO (Briggs, 2011).

PAR was measured with a LI-COR cosine PAR on the float and a Biospherical scalar PAR on the ship's CTD Rosette frame. Both instruments were factory calibrated prior to the experiment, with NIST traceable calibration lamps; the data reported here are based on factory calibrations only. The float made a single daily vertical profile (~ noon/early afternoon); PAR from this profile was used to derive the diffuse attenuation coefficient, K_D, using all data > 10 μmol photons m^{-2} s^{-1}. K_D was applied to all measurements of PAR acquired during the float's mixed-layer drift mode and extrapolated to the surface to produce hourly subsurface PAR fields from which daily isolumes were computed. The isolume of 0.415 mol photons m^{-2} d^{-1} is taken as the radiation level below which net photosynthesis does not occur (Letelier et al., 2004; Boss and Behrenfeld, 2010), and is hereafter referred to as the 0.415 isolume.

2.3 Water samples and laboratory analyses

Water samples were collected from the CTD upcast with 10 L Niskin bottles mounted on the CTD Rosette. Samples for nitrate plus nitrite, hereafter referred as to nitrate, and silicic acid, Si, were collected directly from Niskin bottles into acid-washed LDPE bottles, pre-rinsed three times with sample (Kallin et al., 2011). Unfiltered water samples were frozen immediately after collection and stored at -20º C for up to 8 mo. Samples were thawed in the dark prior to analysis and vigorously vortexed (Gordon et al., 1992) prior to absorptiometric analysis on a Lachat Quickchem 8000 Flow Injection Analysis System (Lachat, 1996, 1999). In addition to quality control of the Lachat output spectra, profiles of Si and nitrate concentrations were examined following the recommendation of the IODE workshop on quality control of chemical oceanographic data (IOC, 2010).

Water samples for pigments and spectral absorption coefficients were filtered through Whatman GF/F filters. Samples for fluorometric analysis of *Chl* were extracted in 5 mL of 90% acetone at -20° C for 24 h and analyzed on a Turner Designs Model 10-AU digital fluorometer that was calibrated before and after the field experiment with Turner Designs *Chl* standards. *Chl* concentrations were calculated following JGOFS protocol (Knap et al., 1996). Filters collected for HPLC pigment analysis were stored in liquid nitrogen until analysis (up to 5 mo). Horn Point Laboratories performed HPLC pigment analyses, using a methanol-based reversed-phase gradient C8 chromatography column system and appropriate standards (Van Heukelem and Thomas, 2001; Hooker et al., 2009). Chl_{HPLC} is the sum of *Chl* plus chlorophyllide *a,* with the latter adjusted to *Chl* equivalent mass (x 893.5/614 molecular mass ratio); the ratio of chlorophyllide-to-Chl_{HPLC} is also reported in *Chl* mass equivalents. Filters collected for particulate spectral absorption coefficients were scanned at sea on a Varian Cary 50 UV-Visible spectrophotometer with a xenon flash lamp and a 1.5 nm slit width, following the Mitchell and Kiefer (1988) method. The filters were extracted in hot methanol and re-scanned to measure residual detrital particulate absorption (Kishino et al., 1985). The difference between the total particulate and detrital absorption coefficients was attributed to the phytoplankton absorption coefficient ($a_{phy}(\lambda)$).

Microbial plankton cell size and numerical concentrations were determined on fresh samples at sea during the May cruise (Sieracki and Poulton, 2011). Cells smaller than 20 μm were analyzed with a flow cytometer (FACScan, BD Biosciences), using *Chl* and phycoerythrin fluorescence as discriminators for three groups of phytoplankton: eukaryotic pico- and nanophytoplankton, cryptophytes, and prokaryotic *Synechococcus spp.* (*Prochlorococcus* was not observed). Heterotrophic microbes were analyzed on separate subsamples and detected using fluorescent stains; heterotrophic bacteria were stained with PicoGreen – Life Technologies Inc. (Veldhuis et al., 1997) and heterotrophic nanoprotists were stained with LysoTracker Green – Life Technologies Inc. (Rose et al., 2004). Cell size for all these groups was determined from forward scatter, where size and scatter relationships were established with microbead size standards and algal cultures of known cell size (Sieracki and Poulton, 2011). Phytoplankton cell carbon was estimated from cell size following the algorithm of Verity et al. (1992). Cells larger than 20 μm were analyzed using a Fluid Imaging Technologies FlowCAM, with image collection triggered by *Chl F*. Four major sub-groups were identified: diatoms, dinoflagellates (autotrophic and

mixotrophic), ciliates, and 'other' microphytoplankton. Biovolume estimates were determined following the method of Sieracki et al. (1989), where particle boundary points were found using the Connected Component Labeling algorithm of Chang et al. (2004), as implemented in Burger and Berge (2008). Cell carbon was calculated from derived biovolumes using the algorithms of Menden-Deuer and Lessard (2000). Heterotrophic microprotists were not enumerated with the FlowCAM, and hence estimates of their carbon biomass missing from analyses of heterotrophic carbon. Total particulate organic carbon (POC) was analyzed as reported in (Cetinić et al., 2012).

2.4 Data analysis and derivation of proxies

Optical data were median filtered (7 point running median) to remove spikes associated with aggregates and other larger particles in the water column (Briggs et al., 2011). Water samples were collected on the upcast, with the CTD held at a constant depth for 60 s before the Niskin bottle closed; only data recorded during the last 30 s before bottle closure were used for analysis. *Chl* samples collected during the *R/V Knorr* cruise were used to convert the ship's FLNTU *Chl F* voltage to *Chl (*µg L^{-1}) using a non-linear best-fit function of temperature, PAR, depth and YD (Figs. 2A, B; n=835; D'Asaro, 2011); this algorithm mostly removed the effects of solar quenching (Fig. 2C) and Si limitation (Section 3.4) on *Chl F*. The resulting *Chl* product converted *Chl F* to *Chl* within an error of 30 – 50% (Figs. 2A, B). This uncertainty, and the lack of PAR sensors on the gliders, caused us to use *Chl F* rather than *Chl* in the subsequent analysis. Glider *Chl F* in digital counts was converted to V, referenced to the ship's FLNTU, based on the inter-calibration procedures; *Chl F* is therefore reported as V for all platforms and the optical community index, *Chl F/*b_{bp}, is reported in units of V m.

In this paper, we focus on properties of the upper water column, i.e., 50 m and shallower. Daytime fluorescence quenching is a ubiquitous phenomenon in surface layers of the ocean, with decreases in *Chl F* caused by photo-inhibitory and/or energy-dependent quenching (Sackmann et al., 2008). *Chl F* normalized to fluorometrically measured *Chl* declined at values of PAR > 100 µmol photon m^{-2} s^{-1} (Fig. 2C). Since 92 % of all PAR values > 100 µmol photon m^{-2} s^{-1} were measured within the top 10 m by both ship and float, we omitted *Chl F* and b_{bp} data collected at depths shallower than 10 m from further analysis for all platforms to avoid potential bias associated with solar quenching of *Chl F*. However, data from water samples (nutrients, HPLC pigments, etc.) collected at all depths shallower than 50 m are included in the analyses.

Principal component analysis (PCA) for assessing potential sources of variability in *Chl F/b_{bp}* was performed on data from 38 CTD profiles from the May cruise. Input parameters for PCA were temperature, mixed layer depth (calculated as the depth at which density differed from the mean density in the top 10 m by < 0.05 kg m^{-3}), depth of the 0.415 isolume, nitrate, Si, *Chl F/b_{bp}* and a term representing diatom dominance of phytoplankton biomass (defined in Section 3.3). A single median value for the upper 50 m was assigned to each parameter for each profile, except for *Chl F/b_{bp}* for which median values were calculated for 10 – 50 m (as explained above). The 0.415 isolume for a given day was derived from float data and assigned to a CTD profile based on YD. Prior to analysis, data were standardized by subtracting the mean and dividing by the standard deviation. Scores of individual data points were scaled by the maximal absolute value of the sample scores and maximal coefficient vector length (Matlab code *biplot.m*).

A "heterogeneity index" for similarity of plankton community composition was calculated based on similarity/dissimilarity of *Chl F/b_{bp}* between pairs of autonomous platforms. The six-hour median value of *Chl F/b_{bp}* between 10 and 50 m was determined for each platform and assigned to one of three optical community groups (as described in Results). These assignments were then compared for each platform pair (total of 10 comparisons). A value of 0 was assigned if the community groups were identical (low heterogeneity) and a value of 1 (high heterogeneity) if they were different. The final heterogeneity index reported for a given time is the average of the 10 comparisons.

3 Results

3.1 The evolution of the spring bloom observed from the Lagrangian float

The evolution and community succession of the spring bloom was measured by the Lagrangian float. Alkire et al. (2012) divided the evolution into six periods based on measured physical and biogeochemical parameters. The float was deployed into a deep wintertime mixed layer with *Chl* < 0.5 μg L^{-1} (the period of *Deep Mixing,* Fig. 3A). During the *Early Bloom* (YD 114 – 119) the mixed layer shoaled from > 100 m to ~ 50 m, approximately the depth of the 0.415 isolume (Fig. 3B); during this period *Chl* exponentially increased to ~ 2 μg L^{-1}. Surface phytoplankton concentration was diluted and net growth was slowed by a storm (*Storm*) which deepened the

mixed layer to ~ 100 m between YD 119 and 123, slightly decreasing near-surface *Chl*. Following the storm, the upper ocean quickly restratified and the mixed layer shoaled above the 0.415 isolume. *Chl* continued to increase during the *Main Bloom* (YD 124 – 134). Beginning around YD 126, spikes below 200 m in *Chl F* and b_{bp} were observed in ship and glider data, as well as in ship c_p data, indicating the onset of a flux event of sinking diatom aggregates (Briggs et al., 2011). *Chl* reached a maximal value of 4.6 μg L^{-1} on YD 133 and shortly thereafter abruptly declined to a quarter of the peak bloom value, ~ 1 μg L^{-1}, by YD 137. Bloom termination continued into the *Eddy* period; *Chl* remained relatively unchanged during the *Post Bloom* period and until the end of the float mission on YD 146.

3.2 Diel and longer temporal patterns in the optical community index

The optical community index at the location of the float varied over time on both diel and longer time scales; the observed diel variability was due mostly to *Chl F*, with the peak consistently occurring around midnight (Fig. 3A, C, D). Similar diel patterns have been previously observed for both *Chl F* and b_{bp} (Marra, 1997; Loisel et al., 2011). Although the effects of solar quenching on daytime values of *Chl F* (Sackmann et al., 2008) were minimized by removing data from the upper 10 m (Fig. 2C), a small daytime quenching signal remained. The longer term variations in *Chl F*/b_{bp} were considerably larger than the diel and, as shown below, were associated either with shifts in the phytoplankton community composition, i.e., diatom *vs.* pico and nanophytoplankton dominance, or a physiological response of diatoms to Si limitation between YD 133 – 136.

During the *Deep Mixing* period, the optical community index was low and variable (Fig. 3D). Part of this variability may have been due to instrumental noise since both *Chl F* and b_{bp} were small (Fig. 3C). There is insufficient ship data during this period to determine whether the variability was due to real fluctuations in community composition. Starting mid-way into the *Early Bloom*, the optical community index increased and remained high until the end of the *Main Bloom* period. As Si concentrations measured from ship samples dropped below 1 mmol m^{-3} (YD 133 – 136), the optical community index increased to its highest values. It then abruptly decreased by more than a factor of two (end of *Main Bloom*) and remained low (*Eddy* and *Post Bloom)* through the end of the float mission.

Figure 4A shows a scatter plot of *Chl F vs.* b_{bp}; three groupings are evident. Within Groups 1 and 2, *Chl F* and b_{bp} covaried linearly but with different slopes; Group 1: *Chl F*= 53.63 b_{bp} + 0.01; Group 2: *Chl F*= 105.34 b_{bp} - 0.02. The range in b_{bp} was equivalent, indicating that the relationship was not driven by the changes in magnitude of b_{bp}. Group 1 is characteristic of the *Eddy* and *Post Bloom* periods; Group 2 of the *Early* through *Main Bloom* periods. Groups 2 and 3 reflect a biphasic relationship, with a break in the slope at higher values of b_{bp}. The regression intercept for the third group is non-linear and does not pass near zero (regression not shown). Group 3 occurred only in the latter part of *Main Bloom* period.

The frequency histogram in Fig. 4B also illustrates these patterns, with two clearly defined groupings of the optical community index: low (Group 1 is centered on 58 V m) and intermediate (Group 2 is centered on 98 V m). Group 3 is more diffuse. As a way to more clearly separate Groups 2 and 3, a frequency distribution was constructed for YDs 120 – 127, a period when diatoms were clearly dominant and Si was not limiting. The results of this analysis (shown as a dashed gray line in Fig. 4B) confirmed the upper limit of the optical community index for Group 2 as 120 V m. Indices in excess of 120 V m were classified as Group 3. Cetinić et al. (2012) refers to Group 1 as a 'recycling community' comprised primarily of pico- and nanophytoplankton and Groups 2 and 3 as a 'diatom community'; in Section 3.3 we present the justification for these designations, which are used henceforth.

3.3 Optical community index is a proxy for phytoplankton community composition

Ship-based measurements of phytoplankton cell carbon allowed us to establish that changes in *Chl F*/b_{bp} corresponded to changes in phytoplankton community composition. In May, the fraction of diatom cell carbon as a percentage of total autotrophic cell carbon, *% diatom*$_C$, was calculated from flow cytometer and FlowCAM samples. The diatoms were primarily chain formers, belonging to the genera *Chaetoceros*, *Thalassionema* and *Pseudo-nitzschia* (K. Richardson, *pers. comm*.). Coincident measurements of flow cytometer, FlowCAM and HPLC pigments (n=16) were used to create a proxy that converted the mass ratio of fucoxanthin-to-*Chl* (*Fuco/Chl,* g/g) to the fraction of diatom cell carbon. This relationship, shown in Fig. 5A (Type II regression, r^2=0.78, $p<0.01$), allowed us to include all HPLC samples in the analysis of community composition:

$$\%\ diatom_C = 77.36(\pm 9.87) \times Fuco/Chl - 11.31(\pm 4.85)\ . \quad (1)$$

The combined data set, including both the direct *% diatom$_C$* measurements and those derived from (1), was designated as *% diatom$_C$ product* and provided information for a total of 94 individual samples from 42 stations, of which 4 were from early April and 38 from May.

Figure 5B used the *% diatom$_C$ product* to show that the optical community index was low when pico and nanoplankton dominated (Group 1) and high when diatoms dominated (Groups 2 and 3), with a transition at about 80 V m, as in Figs. 3D and 4B. There was no clear distinction between Groups 2 and 3 in terms of percent diatom domination. An alternative visualization of the optical community index also shows that the highest values were associated with diatoms (Fig. 6A). Changes in *Chl F or b_{bp}* were not strongly correlated with variability of % diatom$_C$ (respective r^2 of 0.21 and 0.16, and p of <0.01 and p<0.1). During May, the ratio of *Chl*-to-autotrophic carbon showed a moderate trend of higher ratios associated with diatom-dominated communities (Fig. 5C; Type II regression, r^2=0.55, p<0.01). Here *% diatom$_C$* is used rather than the *% diatom$_C$ product*, since total autotrophic carbon is available only from flow cytometer and FlowCAM samples. Samples from periods when mixed layers were deeper than 70 m were excluded to avoid confounding effects of low light photo-adaption on the *Chl*-to-carbon ratio.

The absolute magnitude of heterotrophic carbon (sum of heterotrophic bacteria and nanoflagellate carbon) varied between 15 and 30 μg L^{-1}. The corresponding percentage of heterotrophic carbon-to-POC varied between ~10 – 25% and was not correlated with the variability observed in the optical community index (Fig. 5D, n=74, Type II regression, r^2=0.07, p>0.01). Thus, the optical community index *Chl F*/b_{bp} varies with the fraction of the planktonic carbon due to diatoms.

3.4 Principal component analysis

PCA of *R/V Knorr* CTD profiles (Fig. 7, *n*=38) also show a separation between recycling and diatom dominated communities. Principal component one (PC 1; 38.5% of variance) is dominated by an inverse relationship of surface temperature with mixed layer depth and nutrient concentrations. However, PC 2, explaining nearly as much of the variance (30.2 %), is nearly parallel to *Chl F*/b_{bp} (i.e., the *Chl F*/b_{bp} vector is nearly vertical in Fig. 7). Most stations with a recycling community (low optical community index) had lower loadings on PC 2, while stations

with a diatom community (high optical community index) had higher loadings. The analysis confirmed that trends observed in *Chl F/b_{bp}* are associated with the proportion of diatoms, as the % *$diatom_C$ product* had the largest loading on the second component (0.66).

Although PC 2 shows no significant difference in the % *$diatom_C$ product* among stations for the two types of diatom communities, i.e., Groups 2 and 3 (n=27; two tailed t-test, $p > 0.05$), PC 1 separated them as a function of nutrient concentration, as shown by the high loadings on Si (0.57). Nitrate was not a limiting factor for phytoplankton growth, decreasing from an initial concentration of > 12 mmol m^{-3} in early April to a minimal value of ~ 8 mmol m^{-3} in late May (Alkire et al., 2012). In contrast, Si was likely limiting to diatoms by the peak of the bloom, decreasing from initial surface concentrations of > 4 mmol m^{-3} in early April to < 1 mmol m^{-3} towards the end of the *R/V Knorr* cruise (Fig. 6B).

3.5 Ancillary analyses

Ancillary analyses of chlorophyllide and phytoplankton UV absorption spectra are also indicative of differences between diatoms *vs.* pico and nanophytoplankton. The highest ratios of chlorophyllide-to-Chl_{HPLC} were measured at CTD stations with high values of *Chl F/b_{bp}* (Fig. 8A). Unfortunately, no HPLC samples were collected next to the float during the period when *Chl F/b_{bp}* was highest. In May some of the phytoplankton absorption spectra exhibited unusual spectra. UV peaks with a ratio of $a_{phy}(\lambda\text{-UV peak})/a_{phy}(676)$ in excess of 2 were correlated with a high optical index, i.e., in excess of 80 V m (Fig. 8B); 18 out of 63 spectra fit this criterion. While most UV peaks were centered between 325 – 330 nm, four samples associated with Group 3 had up to seven-fold higher peak heights with maxima shifted to lower wavelengths (310 – 320 nm), increased absorption at 412 nm and reduced absorption at 437 and 467 nm peaks.

3.6 Patchiness of phytoplankton communities

The evolution of the diatom spring bloom, its demise and transition to a pico- and nanophytoplankton community was assessed over a two-month period for the float and four gliders. Both the optical community index and mixed layer depths showed some spatial variability (Figs. 9A, B), likely reflecting submesoscale variability as well as variability in the timing of the diatom bloom initiation and termination. During the bloom peak in May, the *R/V Knorr* carried out a series of bow-tie sampling patterns and the optical community index varied

between some of the lowest and highest values as the ship moved in and out of different patches (Fig. 6, YD 130 – 135). The period of greatest heterogeneity in phytoplankton community composition occurred between YD 115 – 137 (Fig. 9C). The strong salinity component in PC 2 (Fig. 7) also reflects this patchiness; the float patch had an anomalously high value of salinity in addition to a high value of the optical community index.

4 Discussion

4.1 Why does the *Chl F*/b_{bp} ratio vary?

High and low values of the optical community index were correlated with diatom-, and pico- and nanophytoplankton-dominated communities, respectively (Figs. 5, 6 and 7). The direct measurement of HPLC pigments and phytoplankton from the flow cytometer and FlowCAM allowed us to create an optical proxy for phytoplankton community composition for this specific period and to apply it to glider and float data to assess community composition over a broader spatial scale (Fig. 9). The question remains, why does this optical index vary as a function of phytoplankton type? Is it strictly taxonomical, or is it based on physiology, or combination of both?

Ratios must be interpreted with caution, as changes could be due either to the numerator, denominator, or both. *Chl F* is a proxy for *Chl*, but with physiological variability associated with solar quenching (Sackmann et al., 2008; Roesler and Barnard, 2014) and nutrient stress (Cleveland and Perry, 1987). However, neither solar quenching nor Si limitation appears to be responsible for the difference in optical community index between Groups 1 and 2. The influence of the former was minimized by the deliberate exclusion of depths less than 10 m. Nitrogen limitation was unlikely, but indications of Si limitation were correlated only with the highest values of *Chl F*/b_{bp} (see Section 4.2, and Figs. 6B and 7). The denominator, b_{bp}, is a function of particle concentration. Although b_{bp} is also influenced by particle size and refractive index (Stramski et al., 2004), the relationship between POC and b_{bp} within the mixed layer during the May NAB 2008 cruise did not vary as a function of plankton community composition (Cetinić et al., 2012), making a change in particle optics an unlikely explanation.

We examined two hypotheses for the observed patterns of the optical community index. First, the relative contribution of heterotrophic carbon to POC and b_{bp} could vary systematically between the different communities. If the contribution of heterotrophs was consistently greater for Group 1, *Chl* F/b_{bp} would be lower. However, heterotrophic (bacteria and nanoprotist) carbon as a percentage of POC was not correlated with the optical community index (Fig. 5D), making it unlikely that heterotrophic carbon was responsible for changes in the ratio. Although heterotrophic protists > 20 μm were not analyzed, their carbon is less than 30% of the heterotrophic nanoprotist carbon at this time of year (Verity et al., 1993) and inclusion of these larger protists would not change the observed trend.

Second, the *Chl*-to-carbon ratio of diatoms could be larger than that of pico and nanophytoplankton, thereby increasing *Chl* F/b_{bp} in the diatom community. In laboratory cultures for the same irradiance, *Chl* per cell volume scales inversely with cell size (cf. Fujiki and Taguchi, 2002), resulting in higher *Chl*-to-carbon ratios for larger cells. Field studies where cell carbon was determined from measurements of cell volume show higher *Chl*-to-carbon ratios for diatom dominated communities in contrast to communities dominated by small phytoplankton (Llewellyn et al., 2005; Putland and Iverson, 2007). In the California Current, observations supported by models also find higher *Chl*-to-carbon ratios for diatoms than picoplankton for similar environmental conditions (Li et al., 2010). Our data revealed the same trend, approximately a factor of two higher ratios of *Chl*-to-autotrophic carbon for samples dominated by diatoms, although with considerable scatter (Fig. 5C). We conclude that differences observed in *Chl* F/b_{bp} between Groups 1 and 2 are primarily due to taxa specific differences in the cellular *Chl*-to-autotrophic carbon ratios and that the optical community index *Chl* F/b_{bp} varies as a function of the fraction of the planktonic carbon due to diatoms. While changes in the *Chl*-to-carbon ratio of individual species do occur in response to changing light, nutrient, and temperature conditions (e.g. Geider, 1987), species succession offers an alternative hypothesis to that of physiological change as the sole explanation for change in phytoplankton *Chl*-to-carbon and hence ratios of *Chl* F/b_{bp} in the field (cf. Behrenfeld et al. 2005).

4.2 Evidence of Si limitation

Analysis by Egge and Aksnes (1992) indicates that diatoms are unlikely to do well in waters with Si concentrations < 2 mmol m^{-3}. In their review of silicon metabolism in diatoms, Martin-

Jezequel et al. (2000) compiled data for the Michaelis-Menten half saturation constant for Si-dependent growth rate; the median half saturation constant for 17 studies was 1.0 mmol m^{-3}. Concentrations of Si at highest values *of Chl F/b_{bp}* were < 1 mmol m^{-3} (Fig. 6B), leading us to suggest that Group 3 represented diatoms whose photosynthetic physiology was limited by Si.

Does Si limitation affect photosynthetic efficiency and *Chl F*? Reduced photosynthetic efficiency is a typical response to limitation by nitrogen, phosphorous and iron due to the structural and functional roles of these elements in photosynthesis. For most species, *Chl* concentration per cell volume decreases with nutrient limitation, while fluorescence normalized to *Chl* concentration increases when nutrients are limiting (Kruskopf and Flynn, 2006). The increase in fluorescence is due in part to an increase in the *Chl*-specific absorption coefficient due to reduced pigmentation and in part to reduced photochemical quenching due to nutrient limitation (Cleveland and Perry, 1987). While Si itself is not directly associated with photosynthesis and relatively few papers report the effect of Si limitation on fluorescence efficiency in diatoms, the available results suggest that Si limitation does reduce photosynthetic efficiency. For Si-limited cultures of the diatom *Thalassisoria weissflogii*, (Lippemeier et al., 1999; Bucciarelli and Sunda, 2003) report a decrease in photosynthetic efficiency (equivalent to F_v/F_m). In a field study in the Iceland Basin and Rockall Trough in May and June 2001, Moore et al. (2005) found F_v/F_m to be correlated with Si concentration, suggesting reduction in photosynthetic capacity in response to Si stress (note, N concentrations in that study were always > 3 μM, but Si concentrations were often < 1 μM). They also found ~ 2 x higher values of F_0/*Chl* associated with low Si concentrations. During the *Main Bloom* period in NAB 2008, enhanced *Chl F* normalized to both b_{bp} (i.e., optical community index) and extracted *Chl* coincided with Si depletion (Figs. 2D, 4A, 6B, 7). During this period Briggs and Gudmundsson (*pers. comm*.) found that rates of net primary productivity based on float diel cycles of optics and oxygen could only be reconciled with photosynthesis vs. irradiance (P–E)-based estimates of productivity if the P–E parameters were reduced with a Michaelis-Menten-like function and a Ks of 1 μM. Hence, we propose that the highest values of *Chl F/b_{bp}* are indicative of diatom Si limitation.

Two other measurements are also suggestive of physiological effects of Si limitation at the end of the diatom bloom. Chlorophyllide is a pigment linked with diatom senescence (Lorenzen, 1967; Jeffrey, 1980; Llewellyn et al., 2008). Although chlorophyllide is noted as a potential extraction artifact (Jeffrey and Hallegraeff, 1987), this pigment has often been used as a marker

for senescent diatoms at the end of diatom blooms in coastal, open ocean, and high latitude environments (Ridout and Morris, 1985; Head and Horne, 1993; Sigleo et al., 2000; Llewellyn et al., 2008). High relative concentrations of chlorophyllide were associated with both Groups 2 and 3, suggesting that diatoms were in transition to senescence. Unusual features in phytoplankton absorption spectra were only found for samples with high optical community indices, including peaks in the UV typically suggestion of MAAs (mycosporine-like amino acids; Fig. 8B). While such UV peaks are often interpreted as MAAs, Llewellyn and Airs (2010) caution that for diatoms, UV absorption peaks can be associated with derivatives of photosynthetic pigments. Since no direct chemical analyses of MAAs were made, the UV peaks may be another indicator of diatom senescence. *In toto,* these observations suggest that as Si became limiting to diatoms, Si limitation was responsible for the highest values of *Chl F*/b_{bp}, as well as the termination of the Main Bloom, leading to subsequent dominance of pico- and nanophytoplankton that do not require Si in the post-bloom community

4.3 Patchiness of phytoplankton communities

The ship, float and gliders carried sensors for *Chl F* and b_{bp} that had been rigorously inter-calibrated, allowing us to directly compare optical measurements across all platforms. The float tracked a parcel of water, within the constraints discussed by Alkire et al. (2012). The gliders tracked the float, typically operating within 50 km of the float, although at the beginning of the experiment strong currents and eddies occasionally swept them further away. The timeline within the float patch showed a steady progression of increasing phytoplankton biomass beginning about YD 110 and continuing through the *Main Bloom* (Fig. 3A). The increase in biomass was accompanied by an increase in the optical community index, reflecting the beginning of the transition from wintertime pico- and nanophytoplankton to spring bloom diatoms (Fig. 3D); within the float patch, the optical index was relatively constant between YD 118 – 132.

Initially, a similar pattern of low biomass was observed in data from all four gliders, but as the bloom progressed more than a five-fold variation was observed on any given day (Mahadevan et al., 2012). Not only was biomass patchy, but the optical community index was also patchy as the gliders (and ship during the May cruise) moved in and out of water parcels with different phytoplankton communities (Figs. 6A, 9A).

Through analysis of glider and model data, Mahadevan et al. (2012), showed that the springtime stratification is due to the action of submesoscale mixed layer eddies that drive a net horizontal transfer of lighter water above heavier water, thereby stratifying the mixed layer. This mechanism generates patches of shallower mixed layers as seen in Fig. 9B, resulting in patchy blooms. They speculated that different species might dominate in different patches, but they referenced patchiness only as biomass. Here we show patchiness in community composition, with the period of highest heterogeneity occurring after YD 115 and persisting for ~ 20 d (Fig. 9C). Our observation is similar to that of d'Ovidio et al. (2010), who used satellite data to determine that submesoscale patches are short-lived (O(weeks)) ecological niches that allow different phytoplankton taxa to bloom.

Our observations raise the question as to the mechanism(s) of the observed patchiness in phytoplankton community composition. Is it a product of temporal offsets in bloom evolution in the various patches, related to restratification by submesoscale mixed layer eddies, or potential nutrient injection (Levy et al., 2012)? Or to a lack of diatom bloom development in some water parcels, perhaps due to zooplankton patchiness or insufficient diatom seed populations? Or a combination of controlling factors? The float patch appeared to have persisted for the longest time period as a diatom community, although at least one glider briefly observed a diatom patch after the bloom terminated at the float (yellow dots on YD 147-148). The mechanism for diatom bloom termination might also differ among the different patches, controlled by patch-specific abiotic and biotic factors. One mechanisms of diatom bloom termination observed on board the ship was resting spore formation and sinking (Rynearson et al., 2013). This appeared to be widespread as judged by the dominance of these spores in sediment traps at depth. Regardless, from YD 140 to the end of the float mission 5 days later, all five autonomous platforms observed only the single phytoplankton community, i.e., Group 1.

5 Conclusions

Simple optical measurements made from autonomous platforms allow us to follow the variability in phytoplankton biomass (*Chl F*) and POC concentration (b_{bp}) on highly resolved spatial and temporal scales. The ratio of these optical measurements provides additional, more qualitative information about the plankton community composition. The interpretation of these ratios must

be based on *in situ* validation and used within a limited set of conditions, at least until a better mechanistic understanding is developed. In late April the increase in the ratio *Chl F/*b_{bp} signaled a transition from a winter phytoplankton community dominated by pico- and nanophytoplankton to an early spring community dominated by diatoms. The observed shift in the optical index was primarily driven by the change in phytoplankton composition and distribution of biomass, reflecting differences in taxa-specific chlorophyll-to-autotrophic carbon ratios Furthermore, the optical index allowed us to observe changes in the physiological status of the community as well, clearly isolating the senescent, Si-limited, termination stage of the diatom bloom from surrounding patches of diatoms not yet in senescence. However, the changes in *Chl F/*b_{bp}, and by implication the transition in community composition, was not simultaneous over the spatial domain surveyed by the ship and gliders. The application of the optical index demonstrated that mesoscale and submesoscale variability in physical structures is reflected not only in total biomass, but in community composition as well. Although our analysis did not manage to resolve the primary drivers of the observed spatial patchiness in community composition, the optical ratio approach offers a new tool set to study plankton patchiness *in-situ* on temporal and spatial scales relevant to ecosystem and biogeochemical research.

Acknowledgements

We thank Katherine Richardson for species data, Giorgio Dall'Olmo, Andrea Drzewianowski, Kristinn Gudmundsson, Emily Kallin, Eric Rehm, Michael Sauer, and Toby Westberry for help at sea and analyses, the University of Washington's Applied Physics Lab Seaglider group, and the captain, crew and technicians of the *R/V Knorr* and *R/S Bjarni Saemundsson*. This research was funded by the U.S. National Science Foundation (Grants OCE-0628107 and OCE-0628379) and NASA (Grants NNX-08AL92G and NNX-10AP29H).

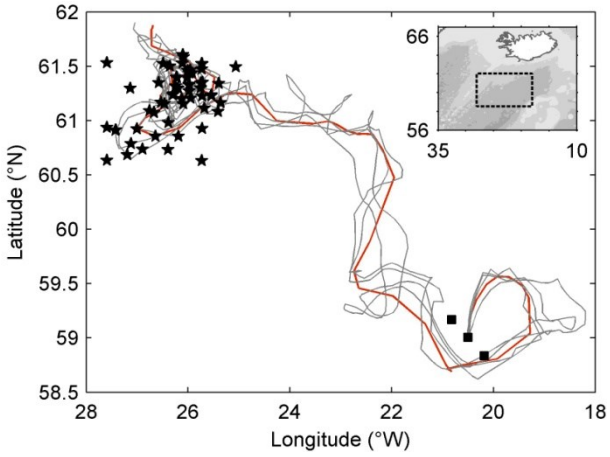

Figure 1. Map of NAB 2008 study area with the Lagrangian float path (red line) and four Seaglider paths (gray lines). Autonomous platforms were deployed during the *R/S Bjarni Saemundsson* cruise in early April 2008; squares indicate ship stations. Additional ship samples were collected on a process cruise on the *R/V Knorr* in May 2008 (stars). Inset map indicates study location relative to Iceland.

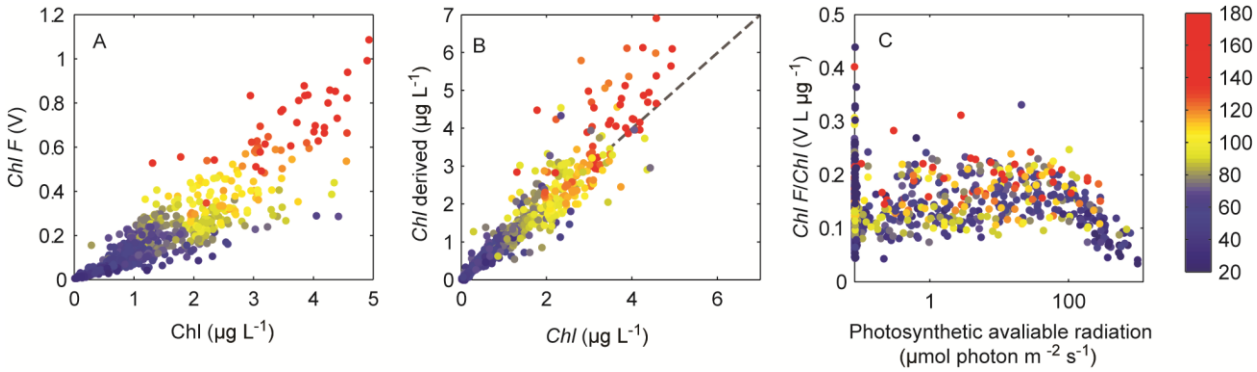

Figure 2. Chlorophyll data from *R/V Knorr* CTD profiles in May, color coded by the optical community index, *Chl* F/b_{bp} (color bar on right; units are V m). (A) *Chl F* vs. extracted chlorophyll concentration, *Chl*, was used to develop a non-linear best-fit function of temperature, PAR, depth and YD for converting float *Chl F* to *Chl* (D'Asaro, 2011). (B) Best-fit derived *Chl* vs. extracted *Chl* shows deviation at higher concentrations (1:1 gray dashed line). (C) *Chl F* normalized to *Chl* exhibits photoquenching at high PAR (surface samples).

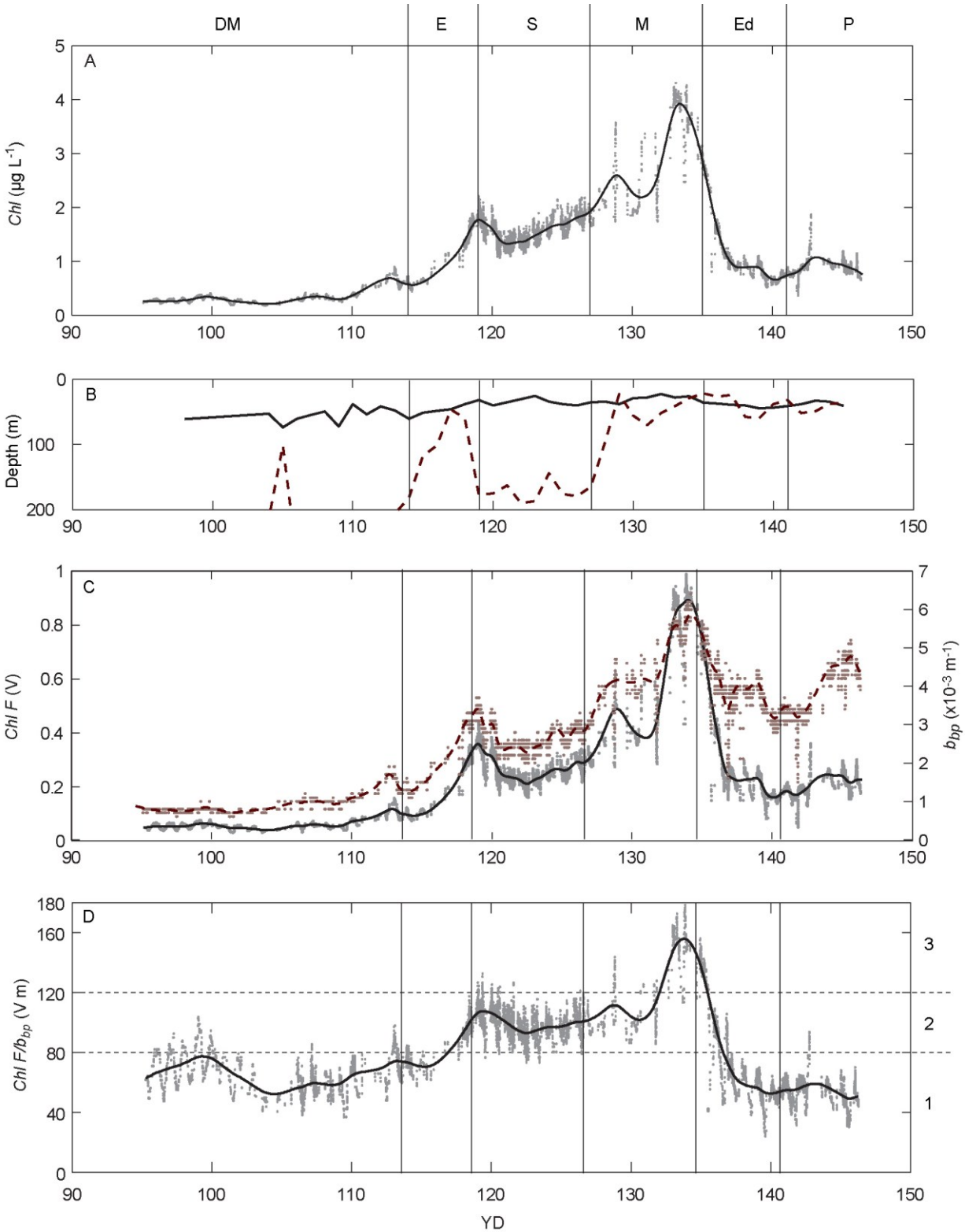

Figure 3. Float data collected for 10 – 50 m for YD 95 –146 (4 April to 25 May 2008). Vertical lines and letters indicate periods in bloom evolution (see section 3.1); DM – *Deep Mixing*, E – *Early Bloom*, S – *Storm*, M – *Main Bloom*, Ed – *Eddy*, P – *Post Bloom*. Dots represent initial

median filtered data (7 point running median); superimposed line is smoothing spline fit (Matlab code *spaps.m*, smoothing parameter 0.1). (A) *Chl* derived from *Chl F*. (B) Mixed layer depth (dashed line) and depth of 0.415 mol photons m^{-2} d^{-1} isolume (solid line). (C) *Chl F* (solid line) and b_{bp} (heavy solid line). (D) Optical community index, *Chl F*/b_{bp}. Horizontal dashed lines indicate transitions between Groups 1 – 2 and 2 – 3. Also see Fig. 6.

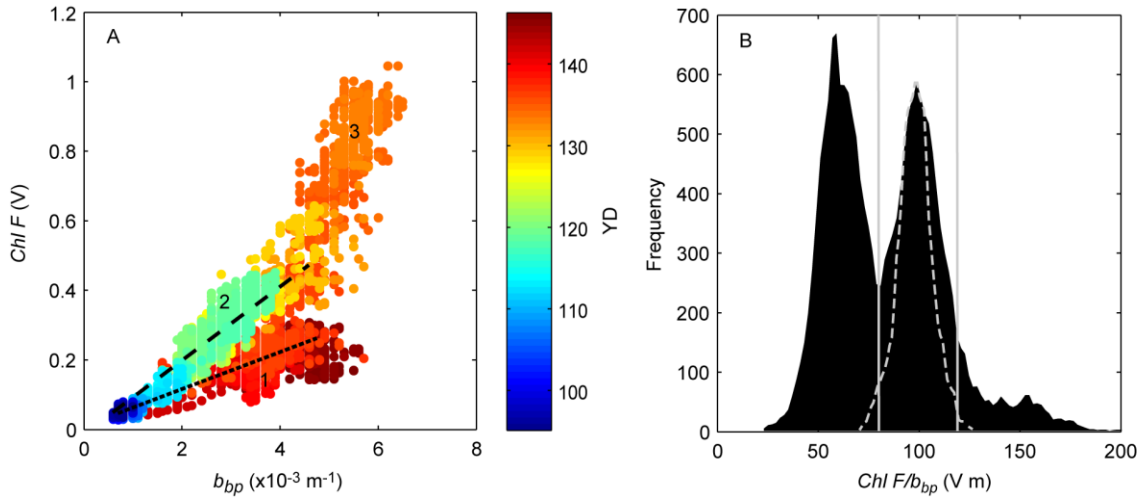

Figure 4. Optical community index and its components from entire float deployment; data from 10 – 50 m. (A) *Chl F* vs. b_{bp} shows three groups: Group 1 (dotted line); Group 2 (dashed line); Group 3, no regression calculated. Some data points in Group 3 are obscured by Group 2. Color coding is YD. (B) Frequency distribution of the optical community index (additional 2 point median filter). Centroids corresponding to the regression lines in panel A. Gray dashed line corresponds to the frequency distribution of the optical community index during period YD 120 – 127.

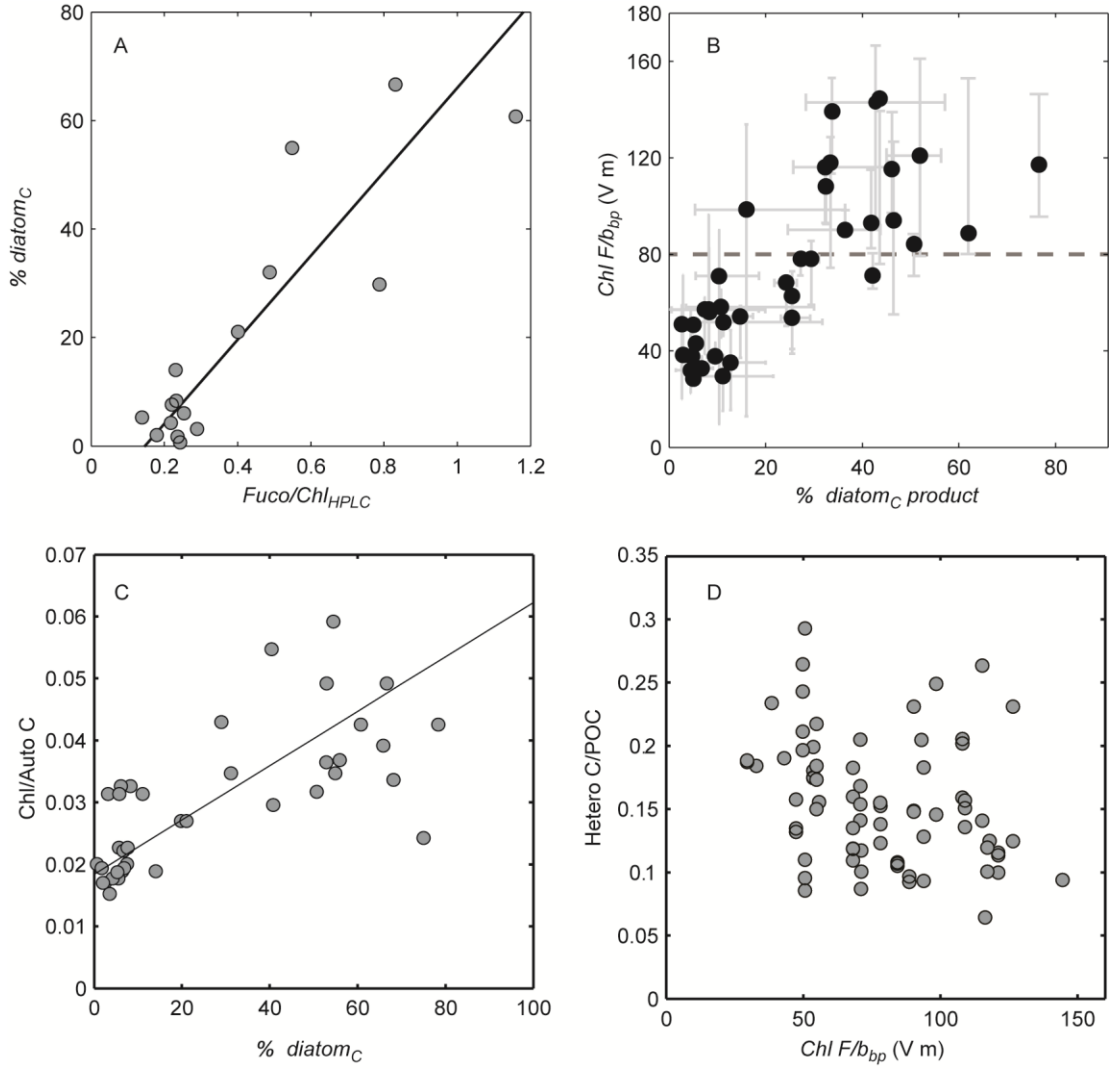

Figure 5. Community composition. Gray circles in Panels A, C and D are for individual water samples; black circles in Panel B are averages for each profile. (A) *Fuco/Chl*$_{HPLC}$ (g/g) is correlated with % *diatom*$_C$. (B) Optical community index is related to phytoplankton community composition, represented as *% diatom*$_C$ *product.* Bars are the range of individual values within each profile; horizontal line indicates the division between Groups 1 and 2 based on Fig. 4B. (C) *Chl*-to-autotrophic carbon increases with the fraction of diatoms. (D) Ratio of heterotrophic carbon biomass to total POC is not correlated with optical community index.

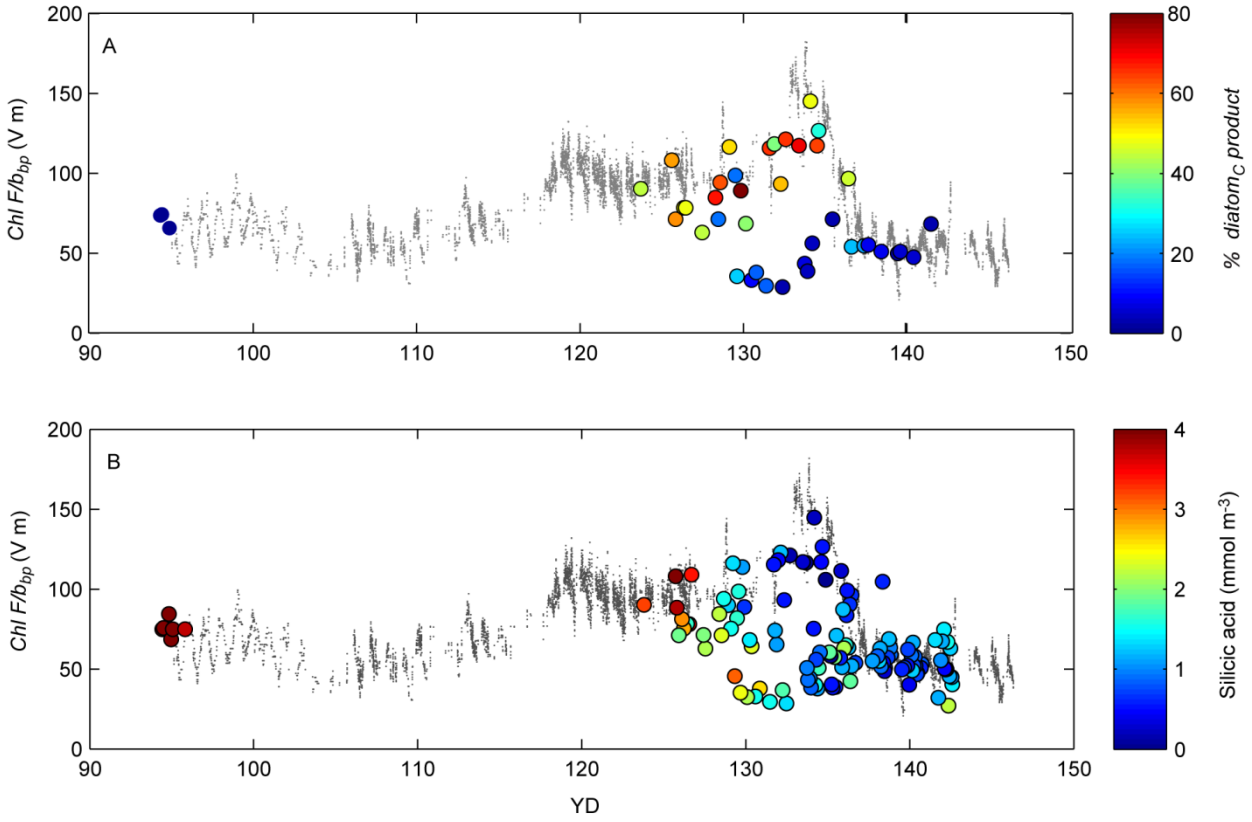

Figure 6. Optical community index, *Chl* F/b_{bp}, from ship CTD profiles (circles) superimposed on float data (gray); 10 – 50 m median is plotted for each ship profile. (A) The optical community index color coded by % $diatom_C$ *product* (n=42). The index was high when the relative diatom abundance was high. (B) Same but color coded by Si concentration. Highest values of *Chl* F/b_{bp} were concurrent with lowest values of Si (n = 123).

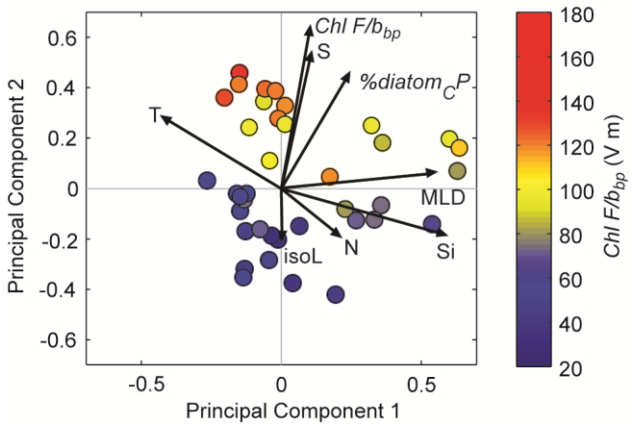

Figure 7. PCA biplot for *R/V Knorr* CTD stations (n = 38), color coded by median *Chl F/ b_{bp}* for 10-50 m, where blue corresponds to Group 1, yellow to Group 2 and red to Group 3. Together PCs 1 and 2 explain 68.7% of the variance. The length of a single parameter vector (black line with arrow) describes its contribution to the PC, while the direction of the vector, starting from the axes intersection, depicts the "biplot" gradient of the specific parameters: T – temperature, S – salinity, IsoL – 0.415 isolume depth, MLD – mixed layer depth, N – nitrate, Si – silicic acid, *Chl F/b_{bp}* – optical community index, and % *$diatom_C$P* (here representing % *$diatom_C$ product* for brevity).

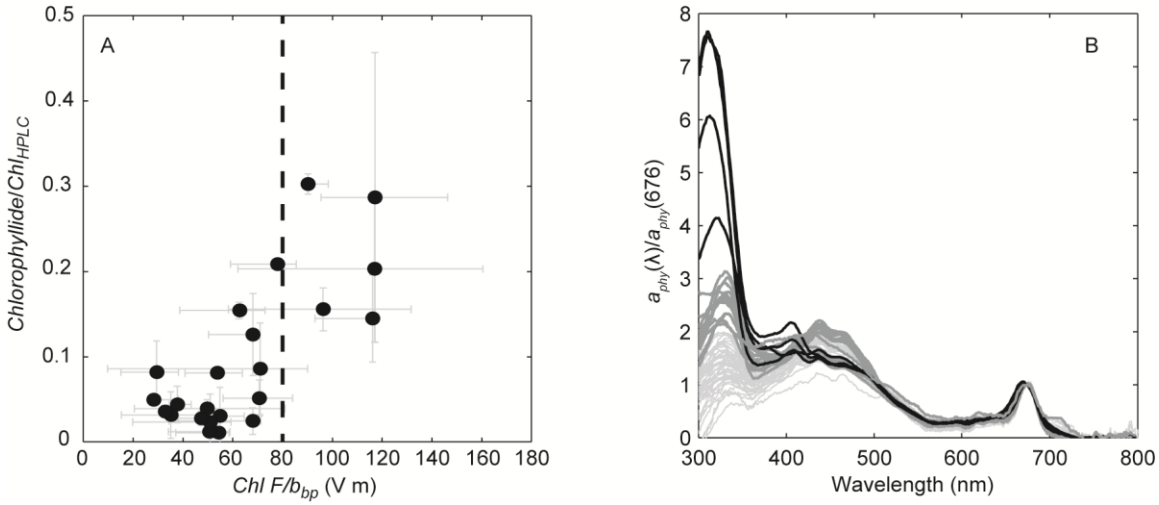

Figure 8. (A) Chlorophyllide concentration normalized to Chl_{HPLC} (g/g) was greater at higher values of the optical community index. Bars are the range of individual samples within each profile (23 profiles, 60 HPLC samples). (B) Phytoplankton absorption coefficient, a_{phy}, normalized to absorption at 676 nm; all available data are shown for completeness (n=63). Large peaks near 300 nm occurred when the optical community index exceeded 80 V m (dark grey and black lines); black lines note spectra with shifts in the absorption peak from 325 – 330 nm to 310 – 315 nm.

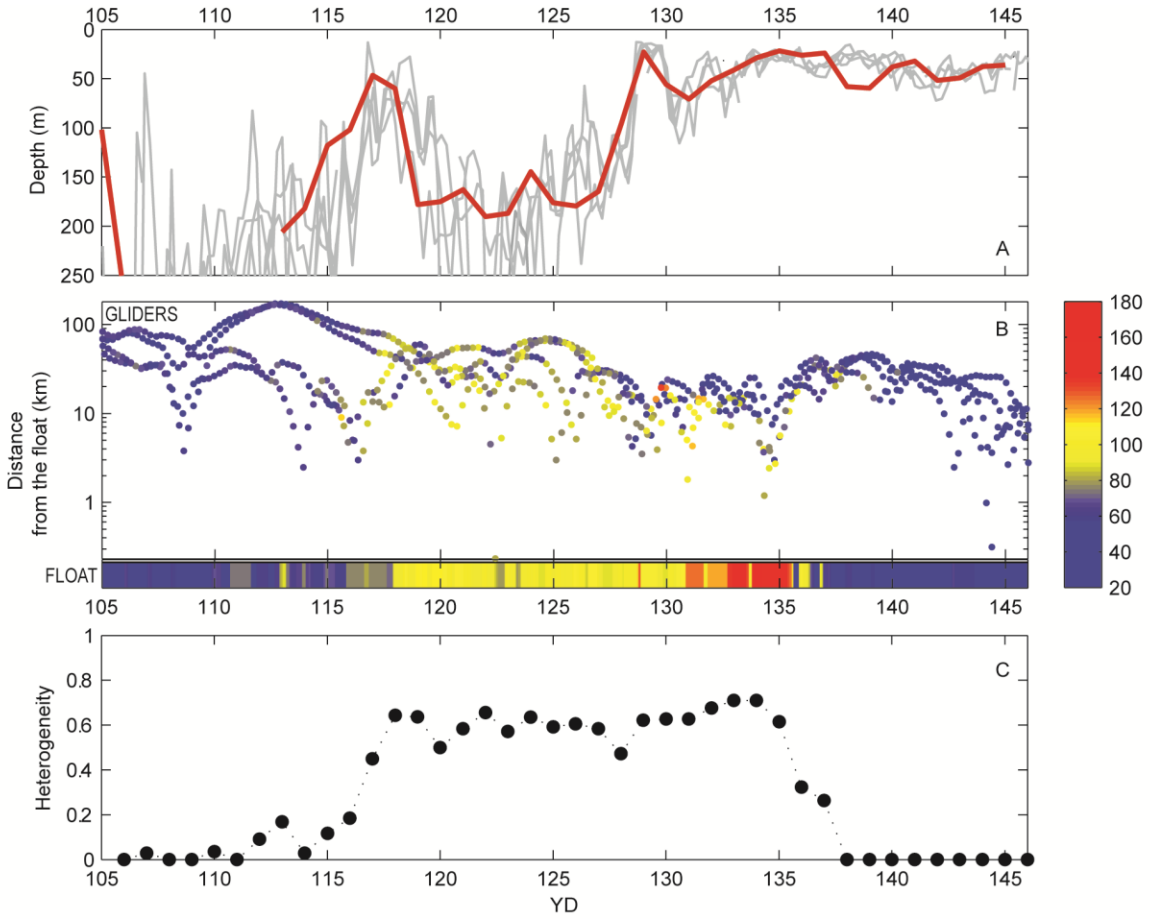

Figure 9. Spatial heterogeneity in phytoplankton community composition, determined from four gliders and the float. (A) Mixed layer depths, from gliders (gray line) and float (red line). (B) Distances between gliders and Lagrangian float. Data are color coded as *Chl F/*b_{bp}; dots represent glider data and color bar at bottom represents float data. (C) Heterogeneity index for community composition, defined in Section 2.4.

1 Table 1. List of measured variables and methodologies, as measured on different platforms. .

Parameter measured	**Symbol /Acronym**	**Instrument or method for specific platform**		
		Ship	*Lagrangian Float*	*Seagliders*
Temperature, Conductivity (Salinity)	T, S	SBE 911*plus*	SBE 41	unpumped, custom SBE CT sensor
Chlorophyll fluorescence	*Chl F*	WET Labs FLNTU	WET Labs FLNTU	WET Labs BB2F
Volume scattering function, calculated optical backscattering	$\boldsymbol{\beta}$(700 nm), b_{bp}	WET Labs FLNTU	WET Labs FLNTU	WET Labs BB2F
Photosynthetically active radiation	PAR	Biospherical QSP2300	LI-COR 192-SA	
Nutrients: nitrate and silicic acid	N, Si	Kallin et al. (2011), Lachat (1996, 1999)	ISUS (not reported)	
Chlorophyll from extracts	*Chl*	Knap et al. (1996)		
Chlorophyll, HPLC analysis	Chl_{HPLC}	Van Heukelem and Thomas (2001), Hooker et al. (2009)		
Phytoplankton absorption coefficient	$a_{phy}(\lambda)$	Mitchell and Kiefer (1988), Kishino et al., (1985)		
Phytoplankton cell carbon		Sieracki and Poulton (2011) and references therein		
Particulate organic carbon	POC	Cetinić et al. (2012)		

2

3

References

Alkire, M. B., D'Asaro, E., Lee, C., Perry, M. J., Gray, A., Cetinic, I., Briggs, N., Rehm, E., Kallin, E., Kaiser, J., and Gonzalez-Posada, A.: Estimates of net community production and export using high-resolution, Lagrangian measurements of O-2, NO3-, and POC through the evolution of a spring diatom bloom in the North Atlantic, Deep-Sea Research Part I-Oceanographic Research Papers, 64, 157-174, 10.1016/j.dsr.2012.01.012, 2012.

Behrenfeld, M. J., Boss, E., Siegel, D. A., and Shea, D. M.: Carbon-based ocean productivity and phytoplankton physiology from space, Global Biogeochemical Cycles, 19, -, 2005.

Boss, E., and Behrenfeld, M.: In situ evaluation of the initiation of the North Atlantic phytoplankton bloom, Geophysical Research Letters, 37, L18603, 10.1029/2010gl044174, 2010.

Bricaud, A., Babin, M., Morel, A., and Claustre, H.: Variability in the Chlorophyll-Specific Absorption-Coefficients of Natural Phytoplankton - Analysis and Parameterization, Journal of Geophysical Research-Oceans, 100, 13321-13332, 1995.

Briggs, N.: Backscatter_Calibration-NAB08, http://osprey.bcodmo.org/dataset.cfm?id=13820&flag=view Biol. and Chem. Oceanogr. Data Manage. Office, Woods Hole, Mass., 2011.

Briggs, N., Perry, M. J., Cetinic, I., Lee, C., D'Asaro, E., Gray, A., and Rehm, E.: High-resolution observations of aggregate flux during a sub-polar North Atlantic spring bloom, Deep Sea Research Part I: Oceanographic Research Papers, 58, 1031-1039, 10.1016/j.dsr.2011.07.007, 2011.

Bucciarelli, E., and Sunda, W. G.: Influence of CO2, nitrate, phosphate, and silicate limitation on intracellular dimethylsulfoniopropionate in batch cultures of the coastal diatom Thalassiosira pseudonana, Limnology and Oceanography, 48, 2256-2265, 2003.

Burger, W., and Burge, M. J.: Digital image processing: an algorithmic introduction using Java, Springer, New York, 2008.

Campbell, L., Henrichs, D.W., Olson, R.J., and Sosik, H.M.: Continuous automated imaging-in-flow cytometry for detection and early warning of *Karenia brevis* blooms in the Gulf of Mexico, Environmental Science and Pollution Research, 20, 6896 – 6902**,** 10.1007/s11356-012-1437-4, 2013.

Cetinić, I., Perry, M. J., Briggs, N. T., Kallin, E., D'Asaro, E. A., and Lee, C. M.: Particulate organic carbon and inherent optical properties during 2008 North Atlantic Bloom Experiment, J. Geophys. Res., 117, C06028, 10.1029/2011jc007771, 2012.

Chang, F., Chen, C. J., and Lu, C. J.: A linear-time component-labeling algorithm using contour tracing technique, Computer Vision and Image Understanding, 93, 206-220, 2004.

Cleveland, J., and Perry, M.: Quantum yield, relative specific absorption and fluorescence in nitrogen-limited Chaetoceros gracilis, Marine Biology, 94, 489-497, 1987.

D'Asaro, E.: Chlorophyll_Calibration-NAB08, http://osprey.bcodmo.org/dataset.cfm?id=13820&flag=view Biol. and Chem. Oceanogr. Data Manage. Office, Woods Hole, Mass. , 2011.

D'Asaro, E. A.: Performance of autonomous Lagrangian floats, Journal of Atmospheric and Oceanic Technology, 20, 896-911, 2003.

d'Ovidio, F., De Monte, S., Alvain, S., Dandonneau, Y., and Lévy, M.: Fluid dynamical niches of phytoplankton types, Proceedings of the National Academy of Sciences, 107, 18366-18370, 10.1073/pnas.1004620107, 2010.

Denman, K. L., and Platt, T.: The variance spectrum of phytoplankton in a turbulent ocean, J. mar. Res, 34, 593-601, 1976.

Ducklow, H. W., and Harris, R. P.: Introduction to the JGOFS North Atlantic bloom experiment Deep-Sea Research Part II Topical Studies in Oceanography, 40, 1–8, 1993.

Egge, J. K., and Aksnes, D. L.: Silicate as Regulating Nutrient in Phytoplankton Competition, Mar Ecol-Prog Ser, 83, 281-289, 1992.

Eriksen, C. C., Osse, T. J., Light, R. D., Wen, T., Lehman, T. W., Sabin, P. L., Ballard, J. W., and Chiodi, A. M.: Seaglider: a long-range autonomous underwater vehicle for oceanographic research, Oceanic Engineering, IEEE Journal of, 26, 424-436, 2001.

Fujiki, T., and Taguchi, S.: Variability in chlorophyll a specific absorption coefficient in marine phytoplankton as a function of cell size and irradiance, J. Plankton Res., 24, 859-874, 10.1093/plankt/24.9.859, 2002.

Geider, R. J.: Light and temperature-dependence of the carbon to chlorophyll-a ratio in microalgae and cyanobacteria - implications for physiology and growth of phytoplankton, New Phytol., 106, 1-34, 10.1111/j.1469-8137.1987.tb04788.x, 1987.

Gordon, L. I., Joe C. Jennings, J., Ross, A. A., and Krest, J. M.: A suggested protocol for continuous flow automated analysis of seawater nutrients (Phosphate, Nitrate, Nitrite and Silicic Acid) in the WOCE Hydrographic Program and the Joint Global Ocean Fluxes Study. 92-1, 1992.

Head, E. J. H., and Horne, E. P. W.: Pigment Transformation and Vertical Flux in an Area of Convergence in the North-Atlantic, Deep-Sea Research Part II-Topical Studies in Oceanography, 40, 329-346, 1993.

Hooker, S. B., Heukelem, L. V., Thomas, C. S., Claustre, H., Ras, J., Schlüter, L., Clementson, L., van der Linde, D., Eker-Develi, E., Berthon, J.-F., Barlow, R., Sessions, H., Ismail, H., and Perl, J.: The Third SeaWiFS HPLC Analysis Round-Robin Experiment (SeaHARRE-3), National Aeronautics and Space Administration, Goddard, 2009.

IOC: First IODE Workshop on Quality Control of Chemical Oceanographic Data Collections, UNESCO, Paris, 2010.

Jeffrey, S. W.: Algal pigment systems, in: Primary productivity in the sea, edited by: Falkowski, P. G., Plenum Publishing Corporation, New York, 33-57, 1980.

Jeffrey, S. W., and Hallegraeff, G. M.: Chlorophyllase Distribution in 10 Classes of Phytoplankton - a Problem for Chlorophyll Analysis, Mar Ecol-Prog Ser, 35, 293-304, 1987.

Kallin, E., Cetinic, I., Perry, M. J., and Sauer, M.: Laboratory_analysis_report-NAB08, http://osprey.bcodmo.org/project.cfm?flag=view&id=102&sortby=project Biol. and Chem. Oceanogr. Data Manage. Office, Woods Hole, Mass. , 2011.

Kishino, M., Takahashi, M., Okami, N., and Ichimura, S.: Estimation of the spectral absorption coefficients of phytoplankton in the sea, Bulletin of Marine Science, 37, 634-642, 1985.

Knap, A., Michaels, A., Close, A., Ducklow, H. and Dickson, A. (eds): Protocols for the Joint Global Ocean Flux Study (JGOFS) Core Measurements. JGOFS Report N. 19, vi + 170 pp. Reprint of the 10C Manuals and Guides No 29, UNESCO 1994, 1996.

Kruskopf, M., and Flynn, K. J.: Chlorophyll content and fluorescence responses cannot be used to gauge reliably phytoplankton biomass, nutrient status or growth rate, New Phytol., 169, 525-536, 10.1111/j.1469-8137.2005.01601.x, 2006.

Lachat, I.: Silicate in brackish or seawater -- QuickChem Method 31-114-27-1-B, Lachat Instruments, Milwaukee, WI, 1996.

Lachat, I.: Nitrate and/or nitrite in brackish or seawater -- QuickChem Method 31-107-04-1-A, Lachat Instruments, Milwaukee, WI, 1999.

Letelier, R. M., Karl, D. M., Abbott, M. R., and Bidigare, R. R.: Light driven seasonal patterns of chlorophyll and nitrate in the lower euphotic zone of the North Pacific Subtropical Gyre, Limnology and Oceanography, 49, 508-519, 2004.

Levy, M., R. Ferrari, P. J.S. Franks, A. P. Martin, and Rivière, P.: Bringing physics to life at the submesoscale, Geophysical Research Letters, 10.1029/2012GL052756, 2012.

Li, Q. P., Franks, P. J., Landry, M. R., Goericke, R., and Taylor, A. G.: Modeling phytoplankton growth rates and chlorophyll to carbon ratios in California coastal and pelagic ecosystems, Journal of Geophysical Research: Biogeosciences (2005–2012), 115, 2010.

Lippemeier, S., Hartig, P., and Colijn, F.: Direct impact of silicate on the photosynthetic performance of the diatom Thalassiosira weissflogii assessed by on- and off-line PAM fluorescence measurements, Journal of Plankton Research, 21, 269-283, 1999.

Llewellyn, C. A., Fishwick, J. R., and Blackford, J. C.: Phytoplankton community assemblage in the English Channel: a comparison using chlorophyll a derived from HPLC-CHEMTAX and carbon derived from microscopy cell counts, Journal of Plankton Research, 27, 103-119, 10.1093/plankt/fbh158, 2005.

Llewellyn, C. A., Tarran, G. A., Galliene, C. P., Cummings, D. G., De Menezes, A., Rees, A. P., Dixon, J. L., Widdicombe, C. E., Fileman, E. S., and Wilson, W. H.: Microbial dynamics during the decline of a spring diatom bloom in the Northeast Atlantic, Journal of Plankton Research, 30, 261-273, 10.1093/plankt/fbm104, 2008.

Llewellyn, C. A., and Airs, R. L.: Distribution and abundance of MAAs in 33 species of microalgae across 13 classes, Marine Drugs, 8, 1273-1291, 2010.

Loisel, H., Vantrepotte, V., Norkvist, K., Meriaux, X., Kheireddine, M., Ras, J., Pujo-Pay, M., Combet, Y., Leblanc, K., Dall'Olmo, G., Mauriac, R., Dessailly, D., and Moutin, T.: Characterization of the bio-optical anomaly and diurnal variability of particulate matter, as seen from scattering and backscattering coefficients, in ultra-oligotrophic eddies of the Mediterranean Sea, Biogeosciences, 8, 3295-3317, 10.5194/bg-8-3295-2011, 2011.

Lorenzen, C. J.: A method for the continuous measurement of the in vivo chlorophyll concentration, Deep-Sea Res, 13, 223-227, 1966.

Lorenzen, C. J.: Determination of chlorophyll and pheo-pigments: spectrophotometric equations, Limnology and Oceanography, 12, 343-346, 1967.

Mahadevan, A., D'Asaro, E., Lee, C., and Perry, M. J.: Eddy-Driven Stratification Initiates North Atlantic Spring Phytoplankton Blooms, Science, 337, 54-58, 10.1126/science.1218740, 2012.

Marra, J.: Analysis of diel variability in chlorophyll fluorescence, Journal of Marine Research, 55, 767-784, 10.1357/0022240973224274, 1997.

Martin-Jezequel, V., Hildebrand, M., and Brzezinski, M. A.: Silicon metabolism in diatoms: Implications for growth, Journal Of Phycology, 36, 821-840, 10.1046/j.1529-8817.2000.00019.x, 2000.

Matrai, P. A., Steele, M., Swift, D., Riser, S., Johnson, K. S., and Breckenridge, L.: Autonomous observations of arctic phytoplankton activity: The first annual cycle in ice-covered waters, International Ocean Colour Science Meeting 2013, Darmstadt, Germany, 2013.

Menden-Deuer, S., and Lessard, E. J.: Carbon to volume relationships for dinoflagellates, diatoms, and other protist plankton, Limnology and Oceanography, 45, 569-579, 2000.

Mitchell, B. G., and Kiefer, D. A.: Chlorophyll a specific absorption and fluorescence excitation spectra for light-limited phytoplankton, Deep-Sea Research, Part 1, 35, 639-663, 1988.

Moisan, T. A., Sathyendranath, S., and Bouman, H. A.: Ocean color remote sensing of phytoplankton functional types, Remote sensing of biomass–principles and applications. Intech, Rijeka, Croatia, 101-122, 2012.

Moore, C. M., Lucas, M. I., Sanders, R., and Davidson, R.: Basin-scale variability of phytoplankton bio-optical characteristics in relation to bloom state and community structure in the Northeast Atlantic, Deep Sea Research Part I: Oceanographic Research Papers, 52, 401-419, 2005.

Munk, W.: Oceanography before, and after, the advent of satellites, Elsevier Oceanography Series, 63, 1-4, 2000.

Nencioli, F., Chang, G., Twardowski, M., and Dickey, T. D.: Optical Characterization of an Eddy-induced Diatom Bloom West of the Island of Hawaii, Biogeosciences, 7, 151-162, 2010.

O'Reilly, J. E., Maritorena, S., Mitchell, B. G., Siegel, D. A., Carder, K. L., Garver, S. A., Kahru, M., and McClain, C.: Ocean color chlorophyll algorithms for SeaWiFS, Journal of Geophysical Research-Oceans, 103, 24937-24953, 1998.

Olson, R. J., and Sosik, H. M.: A submersible imaging-in-flow instrument to analyze nano-and microplankton: Imaging FlowCytobot, Limnol. Oceanogr. Methods, 5, 195-203, 2007.

Perry, M. J., Sackmann, B. S., Eriksen, C. C., and Lee, C. M.: Seaglider observations of blooms and subsurface chlorophyll maxima off the Washington coast, Limnology and Oceanography, 53, 2169-2179, 2008.

Putland, J., and Iverson, R.: Phytoplankton biomass in a subtropical estuary: distribution, size composition, and carbon: chlorophyll ratios, Estuaries and coasts, 30, 878-885, 2007.

Ridout, P., and Morris, R.: Short-term variations in the pigment composition of a spring phytoplankton bloom from an enclosed experimental ecosystem, Marine Biology, 87, 7-11, 1985.

Roesler, C. S., and Barnard, A. H.: Optical proxy for phytoplankton biomass in the absence of photophysiology: Rethinking the absorption line height, Methods in Oceanography, 2014.

Rose, J. M., Caron, D. A., Sieracki, M. E., and Poulton, N.: Counting heterotrophic nanoplanktonic protists in cultures and aquatic communities by flow cytometry, Aquatic Microbial Ecology, 34, 263-277, 2004.

Ryan, J., Greenfield, D., Marin III, R., Preston, C., Roman, B., Jensen, S., Pargett, D., Birch, J., Mikulski, C., and Doucette, G.: Harmful phytoplankton ecology studies using an autonomous molecular analytical and ocean observing network, Limnology and Oceanography, 56, 1255-1272, 2011.

Rynearson, T. A., K. Richardson, R. S. Lampitt, M. E. Sieracki, A. J. Poulton, M. M. Lyngsgaard, and M. J. Perry. Major contribution of diatom resting spores to sinking flux in the sub-polar North Atlantic. Deep-Sea Research, Part I Oceanographic Research Papers. 82:60-71, 2013.

Sackmann, B. S., Perry, M. J., and Eriksen, C. C.: Seaglider observations of variability in daytime fluorescence quenching of chlorophyll-a in Northeastern Pacific coastal waters, Biogeosciences Discuss., 5, 2839-2865, 10.5194/bgd-5-2839-2008, 2008.

Sieracki, M. E., Viles, C. L., and Webb, K. L.: Algorithm to Estimate Cell Biovolume Using Image Analyzed Microscopy, Cytometry, 10, 551-557, 1989.

Sieracki, M. E., and Poulton, N.: Phytoplankton_Carbon-NAB08, http://osprey.bcodmo.org/project.cfm?flag=view&id=102&sortby=project Biol. and Chem. Oceanogr. Data Manage. Office, Woods Hole, Mass. , 2011.

Sigleo, A., Neale, P. J., and Spector, A.: Phytoplankton pigments at the Weddell–Scotia confluence during the 1993 austral spring, Journal of Plankton Research, 22, 1989-2006, 2000.

Sosik, H. M., and Olson, R. J.: Automated taxonomic classification of phytoplankton sampled with imaging-in-flow cytometry, Limnol. Oceanogr. Methods, 5, 204-216, 2007.

Strutton, P. G., Martz, T. R., DeGrandpre, M. D., McGillis, W. R., Drennan, W. M., and Boss, E.: Bio-optical observations of the 2004 Labrador Sea phytoplankton bloom, J. Geophys. Res., 116, C11037, 10.1029/2010jc006872, 2011.

Sullivan, J. M., Twardowski, M., Zaneveld, J. R., and Moore, C.: Measuring optical backscattering in water. *In* A. A. Kokhanovsky (Ed.), *Light Scattering Reviews 7* (pp. 189–224). Springer Berlin Heidelberg, 2013.

Twardowski, M. S., Claustre, H., Freeman, S. A., Stramski, D., and Huot, Y.: Optical backscattering properties of the 'clearest' natural waters, Biogeosciences, 4, 1041-1058, 2007.

Van Heukelem, L., and Thomas, C. S.: Computer-assisted high-performance liquid chromatography method development with applications to the isolation and analysis of phytoplankton pigments, Journal of Chromatography A, 910, 31-49, 2001.

Veldhuis, M. J. W., Cucci, T. L., and Sieracki, M. E.: Cellular DNA content of marine phytoplankton using two new fluorochromes: Taxonomic and ecological implications, Journal Of Phycology, 33, 527-541, 1997.

Verity, P. G., Robertson, C. Y., Tronzo, C. R., Andrews, M. G., Nelson, J. R., and Sieracki, M. E.: Relashionship between cell-volume and the carbon and nitrogen content of marine photosynthetic nanoplankton, Limnology and Oceanography, 37, 1434-1446, 1992.

Verity, P.G., Stoecker, D.K., Sieracki, M.E., Burkill, P.H., Edwards, E.S., and Tronzo, C.R.: Abundance, Biomass and Distribution of Heterotrophic Dinoflagellates During the North-Atlantic Spring Bloom, Deep-Sea Research Part II Topical Studies in Oceanography, 40, 227-244, 1993.

Yoder, J. A., McClain, C. R., Blanton, J. O., and Oey, L. Y.: Spatial scales in CZCS-chlorophyll imagery of the southeastern US continental shelf, Limnology and Oceanography, 929-941, 1987.

Zhang, X., Hu, L., and He, M.-X.: Scattering by pure seawater: Effect of salinity, Opt. Express, 17, 5698-5710, 2009.